Comprehensive Derivation of Small-Signal Model for Virtual-Admittance Based Grid-Forming Modular Multilevel Converters

Comprehensive Derivation of Small-Signal Model for Virtual-Admittance Based Grid-Forming Modular Multilevel Converters

Kavian Kamalinejad
Dept. of Electrical Engineering
Chalmers University of Technology
Göteborg, Sweden
kavian.kamalinejad@chalmers.se

Sohrab Mohtat
Dept. of Electrical Engineering
Chalmers University of Technology
Göteborg, Sweden
sohrab.mohtat@chalmers.se

Amir Reza Zamani
Dept. of Electrical Engineering
Chalmers University of Technology
Göteborg, Sweden
amirz@chalmers.se

***Abstract*—This paper aims to develop an accurate small-signal model of a Grid-Forming Modular Multilevel Converter (GFM-MMC) using a virtual-admittance-based control strategy to establish a general foundation for stability analysis and control design. Yet, the presence of fundamental and second-order harmonics, along with the DC component in the GFM-MMC, complicates the small-signal model derivation. This paper presents a comprehensive framework for modeling and deriving the small-signal model of a GFM-MMC, incorporating fundamental, second-order, and DC components. To achieve this, a time-invariant representation of the converter dynamics is developed using dq-frames synchronized with both the fundamental and second-order harmonic components. The analytically derived input admittance model is then validated through simulation results.**

***Index Terms*—grid-forming control, input-admittance derivation, modular multilevel converter, small-signal modeling.**

I. Introduction

The Modular Multilevel Converter (MMC) is the leading choice for high-power systems, particularly in high voltage direct current transmission [1]. Extensive research has focused on MMC control, with a predominant emphasis on grid-following strategies at the high-level control stage [2]. However, as grid-forming (GFM) control schemes gain attention for providing ancillary services such as inertia support in power systems, their adaptation to MMCs is expected [3].

Due to the significant role of GFM-MMCs in modern power systems, the derivation of their small-signal model becomes essential for analyzing system stability, dynamic performance, and control design. This analysis is critical for assessing stability margins, eigenvalue sensitivity, and the interaction between MMCs and other grid components.

Obtaining the small-signal model of a GFM-MMC, however, could be challenging due to the presence of fundamental and second-order harmonics along with the DC component. Unlike conventional converters, where small-signal modeling only needs to consider the fundamental frequency, MMCs require careful consideration of additional harmonics to accurately capture their dynamic behavior. This introduces additional state variables and coupling effects, making the modeling and linearization process more complex. Therefore, to the best of the authors' knowledge, there is limited literature specifically dedicated to deriving the small-signal model of GFM-MMCs, and more precisely, the derivation of the input admittance of GFM-MMCs. This is important since input admittance serves as a valuable frequency-domain tool for stability assessment [4]. It enables the isolation of a specific part of an overall system contributions to overall system stability [5], which is particularly beneficial in high-order systems. In contrast, other small-signal analysis methods, such as eigenvalues-based stability assessment, do not offer this capability. While some works address related aspects of modeling or analysis of grid-connected MMCs, they often lack a detailed approach to these specific areas. For instance, [6] derives the AC-side input admittance of a grid-connected MMC; however, it does not clearly address the modeling of harmonics of different frequencies. Additionally, the paper considers a grid-following controller for the MMC. In [7], an MMC model in the dq-frame is presented, but its small-signal modeling lacks sufficient detail. Meanwhile, [8] examines a GFM-MMC with power synchronization control but does not incorporate virtual admittance and primarily focuses on eigenvalue analysis rather than frequency-domain analysis. Finally, none of these works clearly address the active power synchronization loop dynamics in small-signal modeling.

This paper aims to provide a comprehensive model of the GFM-MMC, with a focus on the fundamental, second-order, and DC components. By highlighting their roles and interactions, the study offers a clear understanding of how to accurately derive the converter's small-signal model, and consequently, the input admittance of the converter. To achieve this, the converter time-invariant model is represented using dq reference frames synchronized with both the fundamental and second harmonic frequencies.

The rest of the paper is organized as follows: Section II describes the system under study and controllers. Section III presents the time-invariant model of the GFM-MMC, which serves as the foundation for deriving the small-signal model in the following section. The input-admittance of the GFM-MMC is derived in Section IV; moreover, the analytical and

simulation results are compared.

II. System and Controllers Description

This section presents the MMC topology, the averaged model used to derive the equations governing its dynamics, and the GFM control strategy based on virtual admittance for the converter.

A. Modular Multilevel Converter

The grid-connected MMC under study consists of three phase-legs, each containing an upper and a lower arm. Each arm includes N series-connected full-bridge (FB) submodules (SMs) along with a filter reactor characterized by inductance L_{arm} and resistance R_{arm} [9]. A DC power source with voltage of E_{DC} models the pole-to-pole DC voltage of the MMC. The voltages and currents of the upper and lower arms for a single phase-leg are represented as v_{u}, v_{l}, i_{u}, and i_{l}, respectively.

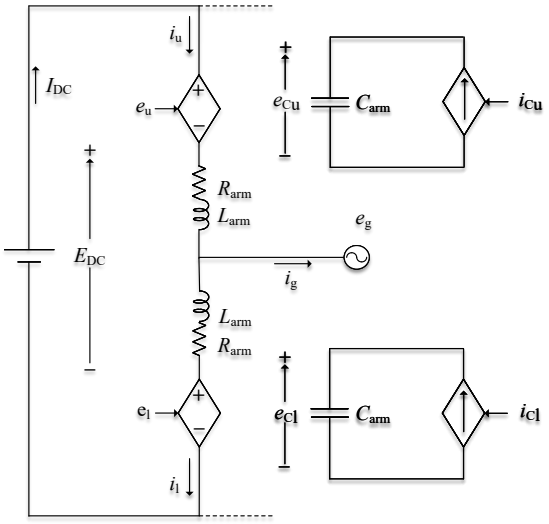

Fig. 1. The averaged model of the MMC for a single phase-leg

As studying the voltage, currents, and switching events of each SM is not of interest in this work, an averaged model of the MMC has been investigated to derive the equations governing its dynamics. To preserve the dynamics of the capacitor voltage while simplifying the analysis, the arm-level averaged model explained in [10] is used in this study. In this model, as depicted for one phase-leg of the MMC in Fig. 1, the series-connected SMs in each arm of the MMC are represented by a controllable voltage source. Moreover, to incorporate the dynamics of the SM capacitor into the MMC's output voltage, a series connection of a controllable current source and the equivalent arm capacitance, given by $C_{\text{arm}} = C/N$, where C is the capacitance of each SM, has been considered. The upper and lower arm currents in Fig. 1 are found to be:

$$i_{\text{u,l}} = \pm\frac{i_{\text{g}}}{2} + i_{\text{cc}} \tag{1}$$

where i_{g} is the current injected into the grid, assumed to contain only the fundamental harmonic component during steady-state operation. This current is regulated by the current controller, with the controller's output voltage being e_{s}. The other component of the arm current is the circulating current i_{cc} and is assumed to be composed of a pure DC current from the DC source (I_{DC}) and a second-order negative-sequence current which is due to the phase mismatch of the capacitor voltage ripple between the upper and lower arms [11]. As this component of the current increases both the losses and the semiconductor rating, it is typically suppressed by a second-order circulating current controller (CCC), with the controller's output being e_{cc}. From (1), the circulating current is found to be $i_{\text{cc}} = (i_{\text{u}} + i_{\text{l}})/2$.

To determine the arm voltages, the upper and lower arm insertion indices of the MMC needs to be defined as following:

$$n_{\text{u,l}} = \frac{\frac{E_{\text{DC}}}{2} \mp e_{\text{s}} - e_{\text{cc}}}{E_{\text{c}}^{\Sigma}} \tag{2}$$

where E_{c}^{Σ} represents the DC value of the sum of the capacitor voltages in the arm. For an MMC with FB SMs, the insertion indices range from -1 to 1 indicating the average number of SMs inserted into the arm of the MMC. The current of the current sources in Fig. 1 is thus defined as:

$$i_{\text{c u,l}} = n_{\text{u,l}} i_{\text{u,l}} \tag{3}$$

Therefore, the arm capacitor voltage is found to be:

$$e_{\text{c u,l}} = \frac{1}{C}\int i_{\text{c u,l}}\, dt \tag{4}$$

The voltage of the arm voltage source in Fig. 1 is determined as:

$$e_{\text{u,l}} = n_{\text{u,l}} e_{\text{c u,l}} \tag{5}$$

The remaining equations of the MMC, which describe the relationships between the grid current (i_{g}) and the circulating current (i_{cc}) with their respective driving voltages, are derived by applying KVL to the circuit in Fig. 1 and are presented as follows [10]:

$$\frac{e_{\text{l}} - e_{\text{u}}}{2} - e_{\text{g}} = \frac{L_{\text{arm}}}{2}\frac{di_{\text{g}}}{dt} + \frac{R_{\text{arm}}}{2} i_{\text{g}} \tag{6}$$

$$E_{\text{DC}} - (e_{\text{u}} + e_{\text{l}}) = 2L_{\text{arm}}\frac{di_{\text{cc}}}{dt} + 2R_{\text{arm}} i_{\text{cc}} \tag{7}$$

B. Grid-Forming Controller

Among the various proposed GFM control strategies, the Virtual-Admittance-based Grid-Forming control (VA-GFM), where the converter appears like a virtual machine with a virtual back electromotive force (EMF) and a virtual impedance, is chosen in this paper. This is due to its advantages in reducing dependence on grid strength. This is achieved by increasing the electrical distance between the point-of-common-coupling (PCC) and the controlled voltage. Additionally, the introduction of virtual inductance and resistance as control parameters, provides more degrees of freedom in controlling the system's performance [12].

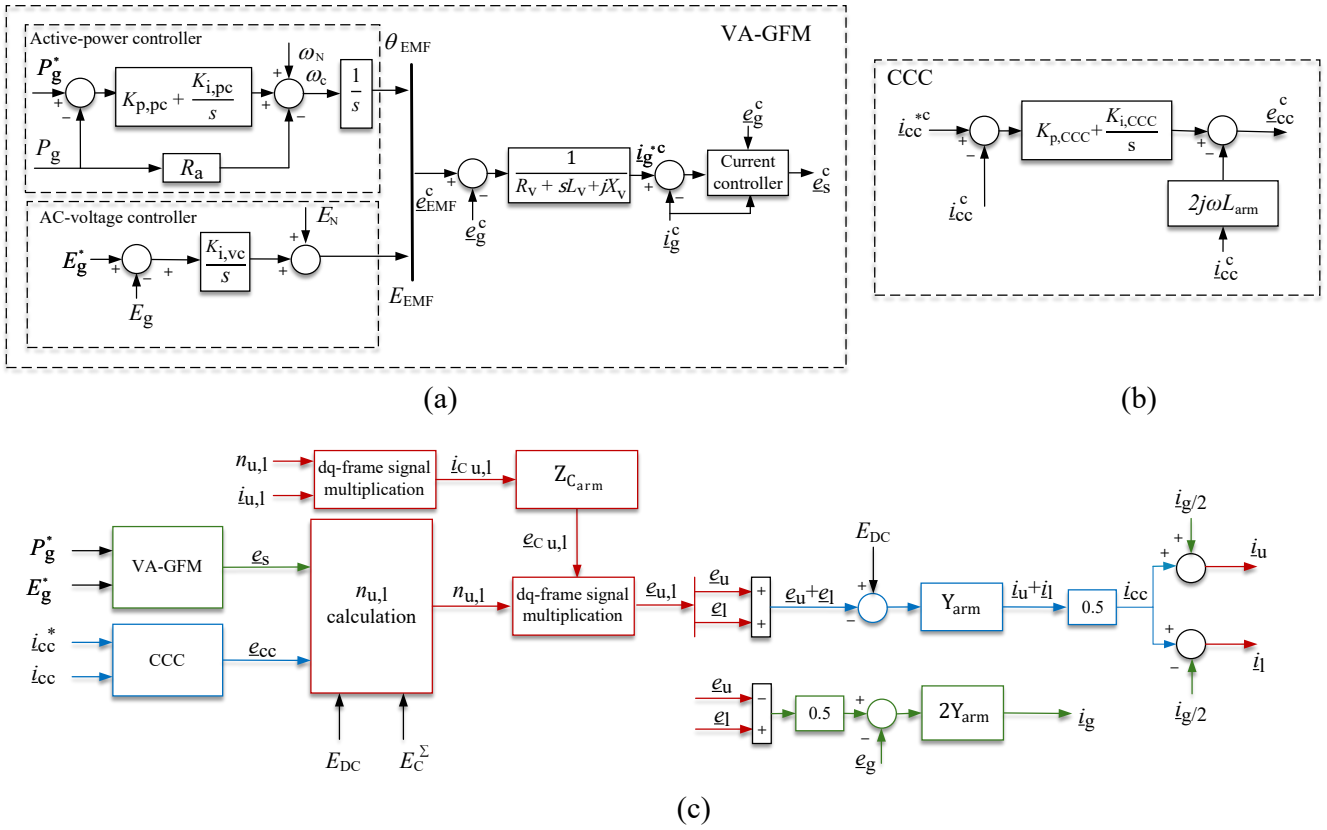

Fig. 2. (a) VA-GFM block diagram. (b) CCC block diagram. (c) Time-invariant model of GFM-MMC.

The synchronization angle θ_{EMF} in VA-GFM is obtained from the active-power controller as:

$$\theta_{\mathbf{EMF}} = \frac{1}{s}[(K_{\mathrm{p,pc}} + \frac{K_{\mathrm{i,pc}}}{s})(P_{\mathrm{g}}^{\star} - P_{\mathrm{g}}) - R_{\mathrm{a}}P_{\mathrm{g}} + \omega_{\mathrm{N}}] \quad (8)$$

where ω_{N} is rated angular frequency (in rad/s) of the AC grid. Moreover, P_{g} and $P_{\mathrm{g}}^{\star}$ are the injected active power and its reference, respectively. $K_{\mathrm{p,pc}}$ and $K_{\mathrm{i,pc}}$ denote the proportional and integral gains of the PI regulator, while R_{a} denotes a transient damping term which is included to improve the dynamic performance of the controller. The parameters of the controller are selected in order to obtain a first order closed loop response from $P_{\mathrm{g}}^{\star}$ to P_{g}.

The AC-voltage controller is based on an integrator with the gain of $K_{\mathrm{i,vc}}$, which is used to regulate the magnitude of the voltage at the PCC (E_{g}) to its reference value ($E_g^{\star}$). Moreover, in the block diagram shown in Fig. 2 (a), E_{N} is the rated system voltage. The AC-voltage controller relation can be written as:

$$E_{\mathbf{EMF}} = E_{\mathrm{N}} + \frac{K_{\mathrm{i,vc}}}{s}(E_{\mathrm{g}}^{\star} - E_{\mathrm{g}}) \quad (9)$$

where capital letters signify the amplitude of the vectors.

In VA-GFM strategy, in addition to active-power controller and AC-voltage controller, the virtual impedance should be implemented in the control system as shown in Fig. 2 (a). L_{v} and R_{v} are the virtual inductance and resistance, respectively. In addition, X_{v} is the term coming from abc to dq transformation and is equal to $\omega_{\mathrm{N}}L_{\mathrm{v}}$. The virtual admittance calculates the reference current in converter dq-frame $\underline{i}_{\mathrm{g}}^{\star\mathbf{c}}$, which is the input of the current controller, as:

$$\underline{i}_{g}^{\star\mathbf{c}} = \frac{\underline{e}_{\mathrm{EMF}}^{\mathbf{c}} - \underline{e}_{\mathrm{g}}^{\mathbf{c}}}{R_{\mathrm{v}} + sL_{\mathrm{v}} + jX_{\mathrm{v}}} \quad (10)$$

where the variables with the underline represents vectors and superscript $^{\mathbf{c}}$ represents the vector in converter dq-frame.

The implemented current controller has a classical structure and is based on a PI regulator with cross-coupling cancellation and voltage feed-forward, which is low-pass filtered with the cut-off frequency of α_{ff}. The current controller calculates the output voltage of the VA-GFM as:

$$\underline{e}_{\mathrm{s}}^{\mathbf{c}} = \frac{\alpha_{\mathbf{ff}}}{s + \alpha_{\mathbf{ff}}}\underline{e}_{\mathrm{g}}^{\mathbf{c}} + j\omega_{\mathrm{N}}L_{\mathrm{f}}\underline{i}_{\mathrm{g}}^{\mathbf{c}} + (K_{\mathrm{p,cc}} + \frac{K_{\mathrm{i,cc}}}{s})(\underline{i}_{\mathrm{g}}^{\star\mathbf{c}} - \underline{i}_{\mathrm{g}}^{\mathbf{c}}) \quad (11)$$

where L_{f} is the physical filter inductance and is equal to $\frac{L_{\mathrm{arm}}}{2}$. Moreover, $K_{\mathrm{p,cc}}$ and $K_{\mathrm{i,cc}}$ denote the proportional and integral gains of the PI regulator for the current controller, respectively.

III. Time-invariant Modeling of GFM-MMC

To derive the small-signal model of the system, the time-invariant model is first established. It is worth noting that the modeling approach used in this work can be easily adapted to different GFM control strategies or a half-bridge MMC topology.

Examining the equations of the MMC, it is observed that in steady-state mode of operation, $i_{\mathrm{u,l}}$ in (1) and $n_{\mathrm{u,l}}$ in (2) consist of zero-sequence DC, first-order positive-sequence, and second-order negative-sequence harmonic components which will be referred to concisely as zero-sequence, first-order, and second-order components, respectively. When the CCC is activated, the second-order component in (1) is fully suppressed, leaving only the zero-sequence and first-order components. Consequently, (3) contains zero-sequence, first, second, and third-order harmonic components. However, the third-order harmonic can be neglected due to the relatively low e_{cc}. A similar analysis reveals that $e_{\mathrm{u,l}}$ in (5) consists of zero-sequence, first-order, and second-order components. Moreover, it can be observed that (6) contains only the first-order component, as it serves as the driving voltage for the grid current. In contrast, (7) includes both the zero-sequence and the second-order component, as it governs the circulating current. Finally, all VA-GFM equations are based on first-order component.

As discussed above, the equations governing the GFM-MMC dynamics include zero-sequence, first-order, and second-order components. Based on the harmonic components present in the GFM-MMC equations, the corresponding *dq* (locked at ω_{N}) *dq2* (locked at $-2\omega_{\mathrm{N}}$), and DC components are obtained using the $abc-dq$ transformation. These components are illustrated in Fig. 2 (c), which presents the block diagram of the time-invariant GFM-MMC model. In this figure, different parts of the block diagram are color-coded to indicate their harmonic components. Green represents sections associated with the fundamental frequency (*dq*), blue corresponds to parts involving zero-sequence and second-order harmonics (*dq2*), and red highlights sections that include zero-sequence, fundamental, and second-order components.

It should be noted that in Fig. 2 (c), Y_{arm} and $Z_{\mathrm{C\,arm}}$ represent the arm filter admittance and the impedance of the arm's equivalent capacitor, respectively. In the Laplace domain, these are defined as:

$$Y_{\mathrm{arm}}(s) = \frac{1}{L_{\mathrm{arm}}s + R_{\mathrm{arm}}} \tag{12}$$

$$Z_{\mathrm{C\,arm}}(s) = \frac{1}{C_{\mathrm{arm}}s} \tag{13}$$

In (12) and (13), s is replaced by $s + j\omega_{\mathrm{N}}$ in *dq* frame, $s - 2j\omega_{\mathrm{N}}$ in *dq2* frame, and remains unchanged for the zero-sequence component.

Furthermore, the multiplications in (3) and (5), in *dq*, *dq2*, and zero-sequence reference frames are carried out using the approach introduced in [7]. The time-domain representations of two generic signals, X(t) and Y(t), each composed of a zero-sequence component, a fundamental frequency component, and a second-order harmonic, are given as follows:

$$\begin{aligned} X(t) =& X_0 + X_d\cos(\omega t) + X_q\sin(\omega t) \\ &+ X_{d2}\cos(2\omega t) + X_{q2}\sin(2\omega t) \end{aligned} \tag{14}$$

$$\begin{aligned} Y(t) =& Y_0 + Y_d\cos(\omega t) + Y_q\sin(\omega t) \\ &+ Y_{d2}\cos(2\omega t) + Y_{q2}\sin(2\omega t) \end{aligned} \tag{15}$$

The multiplication result $Z(t) = X(t) \times Y(t)$, which incorporates the zero-sequence component, fundamental frequency, and second harmonic while disregarding the third and fourth harmonic components, is expressed as follows:

$$\begin{aligned} Z(t) =& \underbrace{(X_0Y_0 + \frac{X_dY_d}{2} + \frac{X_qY_q}{2} + \frac{X_{d2}Y_{d2}}{2} + \frac{X_{q2}Y_{q2}}{2})}_{Z_0} \\ &+ \underbrace{\begin{pmatrix} X_dY_0 + X_0Y_d + \frac{1}{2}X_{d2}Y_d + \frac{1}{2}X_{q2}Y_q + \\ \frac{1}{2}Y_{d2}X_d + \frac{1}{2}Y_{q2}X_q \end{pmatrix}}_{Z_d}\cos(\omega t) \\ &+ \underbrace{\begin{pmatrix} X_qY_0 + X_0Y_q - \frac{1}{2}X_{d2}Y_q + \frac{1}{2}X_{q2}Y_d - \\ \frac{1}{2}Y_{d2}X_q + \frac{1}{2}Y_{q2}X_d \end{pmatrix}}_{Z_q}\sin(\omega t) \\ &+ \underbrace{\left(\frac{X_dY_d}{2} - \frac{X_qY_q}{2} + X_{d2}Y_0 + Y_{d2}X_0\right)}_{Z_{d2}}\cos(2\omega t) \\ &+ \underbrace{\left(\frac{X_qY_d}{2} - \frac{X_dY_q}{2} + X_{q2}Y_0 + Y_{q2}X_0\right)}_{Z_{q2}}\cos(2\omega t) \end{aligned} \tag{16}$$

IV. Small Signal modeling of GFM-MMC

In this section, the input admittance of the GFM-MMC is derived using the previously presented time-invariant model. The accuracy of the derived input-admittance is then validated through comparison with the simulation model.

A. Input-admittance derivation

This section highlights the challenging aspects of obtaining the small-signal model.

Firstly, it is worth mentioning that whenever two signals, which can be the d or q terms in the time-invariant form, are multiplied, their small-signal representation can be expressed as follows:

$$xy = X\Delta y + Y\Delta x \tag{17}$$

where the capital letters signify the steady-state value of the component while Δ represents the small-signal perturbation of the component around the steady-state value.

Due to the active-power controller, the converter system operates with two distinct *dq* reference frames: the system *dq* frame and the controller *dq* frame [13]. The system *dq* frame is defined by an ideal phase angle, calculated using the nominal angular frequency and a given initial phase angle, and is designed to match the phase angle produced by the active-power control loop, θ_{EMF}, under steady-state, unperturbed conditions. The controller *dq* frame is directly defined by

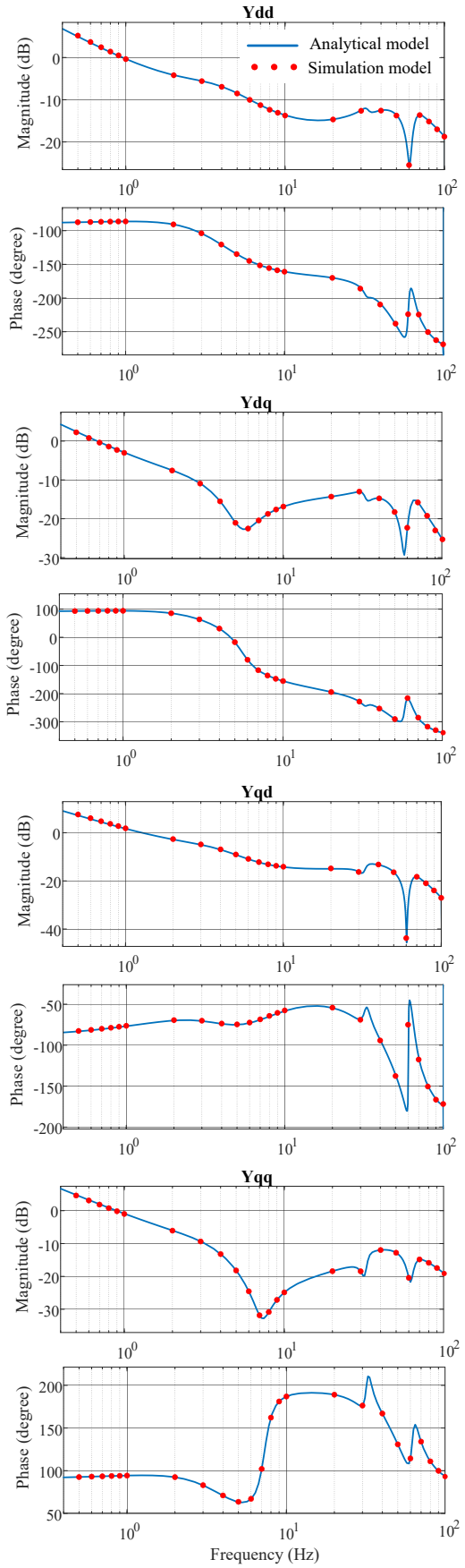

Fig. 3. Validation of GFM-MMC input admittance using analytical and simulation models

θ_{EMF}. Thus, in steady state without perturbations, both frames are aligned. However, small-signal disturbances and transients introduce dynamics in the active-power controller, leading to a misalignment between the frames, defined by the phase angle difference $\Delta\theta$.

To transform a representative vector, $\underline{x}$, between the converter *dq* frame (with superscript ^{c}) and the system *dq* frame (without superscript), equations (18) and (19) are applied as follows [14]:

$$\begin{bmatrix}\Delta x_d^{\mathbf{c}} \\ \Delta x_q^{\mathbf{c}}\end{bmatrix} = \begin{bmatrix}\Delta x_d + X_q n\Delta\theta \\ \Delta x_q - X_d n\Delta\theta\end{bmatrix} \tag{18}$$

$$\begin{bmatrix}\Delta x_d \\ \Delta x_q\end{bmatrix} = \begin{bmatrix}\Delta x_d^{\mathbf{c}} - X_q n\Delta\theta \\ \Delta x_q^{\mathbf{c}} + X_d n\Delta\theta\end{bmatrix} \tag{19}$$

where the value of n is 1 for the signal with the fundamental frequency and -2 for the negative-sequence second-order harmonics.

Furthermore, the small-signal derivation of the voltage controller is as follows:

$$E_{\text{EMF}} = -\frac{e_{gd}^c E_{gd} + e_{gq}^c E_{gq}}{\sqrt{E_{gd}^2 + E_{gq}^2}} \frac{K_{\mathbf{i,VC}}}{s} \tag{20}$$

The remaining parts can be easily linearized, enabling the derivation of the small-signal model of the GFM-MMC using the time-invariant model illustrated in Fig. 2 (c). Then, the input admittance of the converter can be obtained as follows:

$$\begin{bmatrix}\Delta i_{gd} \\ \Delta i_{gq}\end{bmatrix} = -\begin{bmatrix}Y_{dd} & Y_{dq} \\ Y_{qd} & Y_{qq}\end{bmatrix}\begin{bmatrix}\Delta e_{gd} \\ \Delta e_{gq}\end{bmatrix} \tag{21}$$

B. Verification

To validate the analytical model presented in this paper, the derived input admittance is compared with that of the simulation model, with the specifications indicated in Table I. As shown in Fig. 3, the analytical and simulation results exhibit a perfect match, confirming the accuracy of the proposed model.

TABLE I
MMC AND CONTROL PARAMETERS

Parameter	Symbol	Unit
Nominal apparent power	S_{N}	112 MVA (1 pu)
Nominal active power	P_{N}	50 MW
Nominal reactive power	Q_{N}	100 MVAR
Nominal RMS voltage	E_{N}	33 kV (1 pu)
Nominal frequency	f_{N}	50 Hz
Arm filter impedance	Z_{arm}	0.15 pu
Arm filter ratio	$X_{\text{arm}}/R_{\text{arm}}$	20
SM capacitor	C	20 mF
Active power controller bandwidth	α_{pc}	5 Hz
Voltage controller bandwidth	α_{vc}	3 Hz
Active damping term	R_{a}	0.05 pu
Virtual inductance	L_{v}	0.5 pu
Virtual resistance	R_{v}	0.25 pu

V. Conclusion

This paper has presented a detailed modeling approach for deriving the small-signal model of a GFM-MMC. By considering fundamental, second-order, and DC components, a time-invariant representation was developed to accurately capture the converter's dynamic behavior. The model facilitates a deeper understanding of the input admittance characteristics of the GFM-MMC, enabling improved stability analysis and control design. Finally, the derived input admittance was confirmed thorough simulation results.

References

[1] M. A. Perez, S. Ceballos, G. Konstantinou, J. Pou and R. P. Aguilera, "Modular Multilevel Converters: Recent Achievements and Challenges," *IEEE Open Journal of the Industrial Electronics Society*, vol. 2, pp. 224-239, 2021, doi: 10.1109/OJIES.2021.3060791.

[2] S. Mohtat, M. Bongiorno, M. Beza and J. R. Svensson, "Investigation of Pole-to-Pole DC Voltage and Circulating Current on Design Requirements of Full-Bridge Modular Multilevel Converter," *2024 IEEE Energy Conversion Congress and Exposition (ECCE)*, Phoenix, AZ, USA, 2024, pp. 3296-3303, doi: 10.1109/ECCE55643.2024.10860799.

[3] E. Rokrok et al., "Impact of grid-forming control on the internal energy of a modular multilevel converter," 2020 22*nd European Conference on Power Electronics and Applications (EPE'20 ECCE Europe)*, Lyon, France, 2020, pp. 1-10, doi: 10.23919/EPE20ECCEEurope43536.2020.9215646.

[4] J. Sun, "Impedance-Based Stability Criterion for Grid-Connected Inverters," in *IEEE Transactions on Power Electronics*, vol. 26, no. 11, pp. 3075-3078, Nov. 2011, doi: 10.1109/TPEL.2011.2136439.

[5] A. R. Zamani, M. Beza, M. Bongiorno, A. Narula and J. R. Svensson, "Impact of the Reactive Behavior of Grid-Connected Converters on Resonance Stability," *2024 IEEE Energy Conversion Congress and Exposition (ECCE)*, Phoenix, AZ, USA, 2024, pp. 4781-4787, doi: 10.1109/ECCE55643.2024.10861535.

[6] M. Beza, M. Bongiorno and G. Stamatiou, "Analytical Derivation of the AC-Side Input Admittance of a Modular Multilevel Converter With Open- and Closed-Loop Control Strategies," in *IEEE Transactions on Power Delivery*, vol. 33, no. 1, pp. 248-256, Feb. 2018, doi: 10.1109/TPWRD.2017.2701415

[7] A. Jamshidifar and D. Jovcic, "Small-Signal Dynamic DQ Model of Modular Multilevel Converter for System Studies," *IEEE Transactions on Power Delivery*, vol. 31, no. 1, pp. 191-199, Feb. 2016, doi: 10.1109/TPWRD.2015.2478489.

[8] W. Liu, R. Wang, T. Kerekes, T. Dragicevic and R. Teodorescu, "Small Signal Model of Modular Multilevel Converter with Power Synchronization Control," 2023 *IEEE Applied Power Electronics Conference and Exposition (APEC)*, Orlando, FL, USA, 2023, pp. 2815-2820, doi: 10.1109/APEC43580.2023.10131442.

[9] H. Akagi, "Classification, terminology, and application of the modular multilevel cascade converter (MMCC)," *The 2010 International Power Electronics Conference - ECCE ASIA*, Sapporo, Japan, 2010, pp. 508-515, doi: 10.1109/IPEC.2010.5543243.

[10] K. Sharifabadi, et al. "Design, control, and application of modular multilevel converters for HVDC transmission systems," John Wiley & Sons, 2016.

[11] K. Ilves, A. Antonopoulos, S. Norrga and H. -P. Nee, "Steady-State Analysis of Interaction Between Harmonic Components of Arm and Line Quantities of Modular Multilevel Converters," *IEEE Transactions on Power Electronics*, vol. 27, no. 1, pp. 57-68, Jan. 2012, doi: 10.1109/TPEL.2011.2159809.

[12] K. Kamalinejad, A. Narula, M. Bongiorno, M. Beza and J. R. Svensson, "Investigation of Control Parameters' Impact on Damping Property of Grid-Forming Converters," *2024 IEEE Energy Conversion Congress and Exposition (ECCE)*, Phoenix, AZ, USA, 2024, pp. 686-693, doi: 10.1109/ECCE55643.2024.10860863.

[13] L. Harnefors, M. Bongiorno, and S. Lundberg, "Input-admittance calculation and shaping for controlled voltage-source converters," *IEEE Transactions on Industrial Electronics*., vol. 54, no. 6, pp. 3323–3334, Dec. 2007.

[14] B. Wen, D. Boroyevich, R. Burgos, P. Mattavelli and Z. Shen, "Analysis of D-Q Small-Signal Impedance of Grid-Tied Inverters," in *IEEE Transactions on Power Electronics*, vol. 31, no. 1, pp. 675-687, Jan. 2016, doi: 10.1109/TPEL.2015.2398192.